Refined parameters of the HD 22946 planetary system and the true orbital period of planet d

(article starts on next page)

Astronomy & Astrophysics

Refined parameters of the HD 22946 planetary system and the true orbital period of planet d[⋆,⋆⋆]

Z. Garai[1,2,3], H. P. Osborn[4,5], D. Gandolfi[6], A. Brandeker[7], S. G. Sousa[8], M. Lendl[12], A. Bekkelien[12],
C. Broeg[4,25], A. Collier Cameron[13], J. A. Egger[4], M. J. Hooton[4,9], Y. Alibert[4], L. Delrez[10,28], L. Fossati[11],
S. Salmon[12], T. G. Wilson[13], A. Bonfanti[14], A. Tuson[9], S. Ulmer-Moll[4,12], L. M. Serrano[6], L. Borsato[15],
R. Alonso[19,29], G. Anglada[20,30], J. Asquier[18], D. Barrado y Navascues[21], S. C. C. Barros[8,24], T. Bárczy[37],
W. Baumjohann[11], M. Beck[12], T. Beck[4], W. Benz[4,25], F. Biondi[15,33], X. Bonfils[22], M. Buder[17],
J. Cabrera[17], V. Cessa[4], S. Charnoz[23], Sz. Csizmadia[17], P. E. Cubillos[14,44], M. B. Davies[40], M. Deleuil[31],
O. D. S. Demangeon[22,24], B.-O. Demory[25], D. Ehrenreich[12], A. Erikson[17], V. Van Eylen[45], A. Fortier[4,25],
M. Fridlund[26,27], M. Gillon[10], V. Van Grootel[28], M. Güdel[16], M. N. Günther[18], S. Hoyer[31], K. G. Isaak[18],
L. L. Kiss[38], M. H. Kristiansen[46], J. Laskar[32], A. Lecavelier des Etangs[39], C. Lovis[12], A. Luntzer[16],
D. Magrin[15], P. F. L. Maxted[36], C. Mordasini[4], V. Nascimbeni[15], G. Olofsson[7], R. Ottensamer[16], I. Pagano[35],
E. Pallé[19,29], G. Peter[17], G. Piotto[15,34], D. Pollacco[41], D. Queloz[9,12], R. Ragazzoni[15,34], N. Rando[18],
H. Rauer[17,42], I. Ribas[20,30], N. C. Santos[8,24], G. Scandariato[35], D. Ségransan[12], A. E. Simon[4],
A. M. S. Smith[17], M. Steller[11], Gy. M. Szabó[1,2], N. Thomas[4], S. Udry[12], J. Venturini[12], and N. Walton[43]

(Affiliations can be found after the references)

ABSTRACT

Context. Multi-planet systems are important sources of information regarding the evolution of planets. However, the long-period planets in these systems often escape detection. These objects in particular may retain more of their primordial characteristics compared to close-in counterparts because of their increased distance from the host star. HD 22946 is a bright (G = 8.13 mag) late F-type star around which three transiting planets were identified via Transiting Exoplanet Survey Satellite (TESS) photometry, but the true orbital period of the outermost planet d was unknown until now.
Aims. We aim to use the Characterising Exoplanet Satellite (CHEOPS) space telescope to uncover the true orbital period of HD 22946d and to refine the orbital and planetary properties of the system, especially the radii of the planets.
Methods. We used the available TESS photometry of HD 22946 and observed several transits of the planets b, c, and d using CHEOPS. We identified two transits of planet d in the TESS photometry, calculated the most probable period aliases based on these data, and then scheduled CHEOPS observations. The photometric data were supplemented with ESPRESSO (Echelle SPectrograph for Rocky Exoplanets and Stable Spectroscopic Observations) radial velocity data. Finally, a combined model was fitted to the entire dataset in order to obtain final planetary and system parameters.
Results. Based on the combined TESS and CHEOPS observations, we successfully determined the true orbital period of the planet d to be 47.42489 ± 0.00011 days, and derived precise radii of the planets in the system, namely $1.362 \pm 0.040\,R_\oplus$, $2.328 \pm 0.039\,R_\oplus$, and $2.607 \pm 0.060\,R_\oplus$ for planets b, c, and d, respectively. Due to the low number of radial velocities, we were only able to determine 3σ upper limits for these respective planet masses, which are $13.71\,M_\oplus$, $9.72\,M_\oplus$, and $26.57\,M_\oplus$. We estimated that another 48 ESPRESSO radial velocities are needed to measure the predicted masses of all planets in HD 22946. We also derived stellar parameters for the host star.
Conclusions. Planet c around HD 22946 appears to be a promising target for future atmospheric characterisation via transmission spectroscopy. We can also conclude that planet d, as a warm sub-Neptune, is very interesting because there are only a few similar confirmed exoplanets to date. Such objects are worth investigating in the near future, for example in terms of their composition and internal structure.

Key words. methods: observational – techniques: photometric – planets and satellites: fundamental parameters

---

1. Introduction

Multi-planet systems are important from many viewpoints. Not only are they susceptible of relatively straightforward confirmation as bona fide planets (Lissauer et al. 2012), they also allow intra-planetary comparisons to be made for planets which formed under the same conditions; see for example Weiss et al. (2018). The majority of the known multi-planet systems were found by space-based exoplanet transit surveys. This is because, while giant hot-Jupiters are relatively easy to observe with ground-based photometry, the detection of smaller planets, for example, Earths, super-Earths, and sub-Neptunes, which are typically found in multi-planet systems, requires the precise photometry of space-based observatories such as TESS (Ricker 2014).

Mutual gravitational interactions in some multi-planet systems can provide constraints on the planet masses through transit time variations (TTVs); see for example Nesvorný & Morbidelli (2008). Alternatively, radial velocity (RV) observations are needed to put constraints on the masses of planets (Mayor & Queloz 1995). Even where masses cannot be determined, mass upper limits can provide proof that the studied objects are of planetary origin; see for example Stefánsson et al. (2020); Hord et al. (2022), or Wilson et al. (2022). Mass determination can then help constrain the internal structure of the planet bodies, and break degeneracies in atmospheric characterisation follow-up studies. If precise planet radii are also determined from transit photometry, this allows the planet internal density to be calculated and the planetary composition to be estimated; see for example Delrez et al. (2021) and Lacedelli et al. (2021, 2022). Precise planetary parameters also allow the planets to be put in the context of population trends, such as the radius (Fulton et al. 2017; Van Eylen et al. 2018; Martinez et al. 2019; Ho & Van Eylen 2023) and density (Luque & Pallé 2022) valleys.

Long-period planets in multiple-planet systems often escape detection, especially when their orbital periods are longer than the typical observing duration of photometric surveys (e.g. ∼27 days for TESS). However, detecting such planets is also important. For example, the increased distance from their host stars means that, when compared with close-in planets, they may retain more of their primordial characteristics, such as unevaporated atmospheres (Owen 2019) or circumplanetary material (Dobos et al. 2021). Due to the limited observing duration of the TESS primary mission, which observed the majority of the near-ecliptic sectors for only 27 days, planets on long periods produce only single transits. However, thanks to its extended mission, TESS re-observed the same fields 2 yr later, and in many cases was able to re-detect a second transit; see for example Osborn et al. (2022). These 'duotransit' cases require follow-up in order to uncover the true orbital period due to the gap, which causes a set of aliases, $P \in (t_{\mathrm{tr},2} - t_{\mathrm{tr},1})/(1, 2, 3, \ldots, N_{\max})$, where $t_{\mathrm{tr},1}$ and $t_{\mathrm{tr},2}$ are the first and the second observed mid-transit times, respectively. The longest possible period is the temporal distance between the two mid-transit times, $P_{\max} = (t_{\mathrm{tr},2} - t_{\mathrm{tr},1})$, and the shortest possible period is bounded by the non-detection of subsequent transits.

In addition to ground-based telescopes, the CHEOPS space observatory (Benz et al. 2021) can be used to follow-up duotransit targets and to determine their true orbital periods and other characteristics. For example, the periods of two young sub-Neptunes orbiting BD+40 2790 (TOI-2076, TIC-27491137) were found using a combination of CHEOPS and ground-based

Table 1. Log of TESS photometric observations of HD 22946.

Time interval of observation	Sector no.	Transits
HD 22946b		
2018-09-20–2018-10-18	03	5
2018-10-18–2018-11-15	04	6
2020-09-22–2020-10-21	30	6
2020-10-21–2020-11-19	31	6
HD 22946c		
2018-09-20–2018-10-18	03	2
2018-10-18–2018-11-15	04	2
2020-09-22–2020-10-21	30	2
2020-10-21–2020-11-19	31	2
HD 22946d		
2018-10-18–2018-11-15	04	1
2020-09-22–2020-10-21	30	1

photometric follow-up observations (Osborn et al. 2022). Furthermore, these combined observations uncovered the TTVs of two planets, and also improved the radius precision of all planets in the system. CHEOPS observations also recovered orbital periods of duotransits in HIP 9618 (Osborn et al. 2023), TOI-5678 (Ulmer-Moll et al. 2023), and HD 15906 (Tuson et al. 2023) systems. In the present study, we investigated the HD 22946 system with a similar aim. HD 22946 (TOI-411, TIC-100990000) is a bright ($G = 8.13$ mag) late F-type star with three transiting planets. The planetary system was discovered and validated only recently by Cacciapuoti et al. (2022, hereafter C22). The authors presented several parameters of the system, including the radii and mass limits of the planets. They found that planet b is a super-Earth with a radius of $1.72 \pm 0.10\,R_\oplus$, while planets c and d are sub-Neptunes with radii of $2.74 \pm 0.14\,R_\oplus$ and $3.23 \pm 0.19\,R_\oplus$, respectively. The 3σ upper mass limits of planets b, c, and d were determined – based on ESPRESSO spectroscopic observations (see Sect. 2.3) – to be 11 $M_\oplus$, 14.5 $M_\oplus$, and 24.5 $M_\oplus$, respectively. As TESS recorded several transits during observations in sector numbers 3, 4, 30, and 31, the discoverers easily derived the orbital periods of the two inner planets, b and c, which are about 4040 days and 9573 days, respectively. The orbital period of planet d was not found by C22. The authors determined its presence through a single transit found in sector number 4 and obtained its parameters from this single transit event. Its depth and the host brightness make planet d easily detectable with CHEOPS, and therefore HD 22946 was observed several times with this instrument within the Guaranteed Time Observations (GTO) programmes CH_PR110048 and CH_PR100031, with the main scientific goals being to uncover the true orbital period of planet d and to refine the parameters of the HD 22946 system based on CHEOPS and TESS observations via joint analysis of the photometric data, supplemented with ESPRESSO spectroscopic observations of HD 22946.

The present paper is organised as follows. In Sect. 2, we provide a brief description of observations and data reduction. In Sect. 3, we present the details of our data analysis and our first results, including stellar parameters, period aliases of HD 22946d from the TESS data, and a search for TTVs. Our final results based on the combined TESS, CHEOPS, and RV model are described and discussed in Sect. 4. We summarise our findings in Sect. 5.

Table 2. Log of CHEOPS photometric observations of HD 22946.

Visit No.	Start date (UTC)	End date (UTC)	File key	CHEOPS product	Integration time (s)	Number of frames
1	2021-10-17 03:22	2021-10-17 14:40	CH_PR100031_TG021201	Subarray	2×20.0	629
1	2021-10-17 03:22	2021-10-17 14:40	CH_PR100031_TG021201	Imagettes	20.0	1258
2	2021-10-18 08:14	2021-10-18 19:04	CH_PR100031_TG021101	Subarray	2×20.0	637
2	2021-10-18 08:14	2021-10-18 19:04	CH_PR100031_TG021101	Imagettes	20.0	1274
3	2021-10-25 07:08	2021-10-25 19:49	CH_PR110048_TG010001	Subarray	2×20.4	708
3	2021-10-25 07:08	2021-10-25 19:49	CH_PR110048_TG010001	Imagettes	20.4	1416
4	2021-10-28 02:12	2021-10-28 13:50	CH_PR110048_TG010101	Subarray	2×20.4	666
4	2021-10-28 02:12	2021-10-28 13:50	CH_PR110048_TG010101	Imagettes	20.4	1332
5	2021-10-29 08:48	2021-10-29 18:14	CH_PR100031_TG021202	Subarray	2×20.0	555
5	2021-10-29 08:48	2021-10-29 18:14	CH_PR100031_TG021202	Imagettes	20.0	1110

Notes. The time interval of individual observations, the file key, which supports fast identification of the observations in the CHEOPS archive, type of the photometric product (for more details see Sect. 2.2), the applied integration time, co-added exposures at the subarray type CHEOPS product, and the number of obtained frames.

2. Observations and data reduction

2.1. TESS data

HD 22946 was observed during four TESS sectors: numbers 3, 4, 30, and 31 (see Table 1). The time gap between the two observing seasons is almost 2 yr. These TESS data were downloaded from the Mikulski Archive for Space Telescopes[1] in the form of Presearch Data Conditioning Simple Aperture Photometry (PDCSAP) flux. These data, containing 61 987 data points, were obtained from 2-min integrations and were initially smoothed by the PDCSAP pipeline. This light curve is subjected to more treatment than the simple aperture photometry (SAP) light curve, and is specifically intended for detecting planets. The pipeline attempts to remove systematic artifacts while keeping planetary transits intact. The average uncertainty of the PDCSAP data points is 310 ppm.

During these TESS observing runs, 23 transits of planet b were recorded, and the transit of planet c was observed eight times in total (see more details in Table 1). As in C22, we also initially recognised a transit-like feature in the sector number 4 data at $t_{tr,1} = 2\,458\,425.1657$ BJD$_{TDB}$ through visual inspection of the light curve. Given 65%–80% of single transits from the TESS primary mission will re-transit in the extended mission sectors (see Cooke et al. 2019, 2021), we subsequently visually inspected the light curve once the TESS year 3 data were available and found a second dip at $t_{tr,2} = 2\,459\,136.5357$ BJD$_{TDB}$ in the sector number 30 data with near-identical depth and duration. Given the high prior probability of finding a second transit, the close match in transit shape between events, and the high quality of the data (i.e. minimal systematic noise elsewhere in the light curve), we concluded that this signal is a bona fide transit event and that the transits in sector numbers 4 and 30 are very likely caused by the same object, that is, by planet d.

Outliers were cleaned using a 3σ clipping, where σ is the standard deviation of the light curve. With this clipping procedure, we discarded 300 data points out of 61 987, which is ~0.5% of the TESS data. Subsequently, we visually inspected the dataset in order to check the effect of the outlier removal, which we found to be reasonable. As TESS uses as time stamps Barycentric TESS Julian Date (i.e. BJD$_{TDB}$ − 2 457 000.0), during the next step we converted all TESS time stamps to BJD$_{TDB}$.

2.2. CHEOPS data

HD 22946 was observed five times with the CHEOPS space telescope. This is the first European space mission dedicated primarily to the study of known exoplanets. It consists of a telescope with a mirror of 32 cm in diameter based on a Ritchey-Chrétien design. The photometric detector is a single-CCD camera covering the wavelength range from 330 to 1100 nm with a field of view of 0.32 deg^2. The payload design and operation have been optimised to achieve ultra-high photometric stability, achieving a photometric precision of 20 ppm on observations of a G5-type star in 6 h, and 85 ppm observations of a K5-type star in 3 h (Benz et al. 2021). The CHEOPS observations were scheduled based on the existing TESS observations of planets b and c, and mainly based on the observed transit times of planet d (see Sect. 2.1). The marginal probability for each period alias of planet d was calculated using the MonoTools package (see Sect. 3.2). We were not able to observe all the highest-probability aliases, because some were not visible during the two-week period of visibility. Within the program number CH_PR110048, we therefore planned to observe the three highest-probability aliases of planet d with CHEOPS, but due to observability constraints and conflicts with other observations, only two visits[2] of planet d aliases were scheduled. Its true orbital period was confirmed during the second observation. The remaining three visits were scheduled in the framework of the program number CH_PR100031. Based on these CHEOPS observations, three transits of planet b were recorded during visits 1, 3, and 5, the transit of planet c was observed twice during visits 2 and 4, and a single transit of planet d (in multiple transit feature with planet c) was detected during the CHEOPS visit 4. Further details about these observations can be found in Table 2.

From the CHEOPS detector, which has 1024×1024 pixels, a 200×200 pixels subarray is extracted around the target point-spread function (PSF), which is used to compute the photometry. This type of photometry product was processed by the CHEOPS Data Reduction Pipeline (DRP) version 13.1.0 (Hoyer et al. 2020). It performs several image corrections, including bias-, dark-, and flat-corrections, contamination estimation, and background-star correction. The DRP pipeline produces four different light-curve types for each visit, but we initially analysed only the decontaminated 'OPTIMAL' type, where the aperture

---

[1] See https://mast.stsci.edu/portal/Mashup/Clients/Mast/Portal.html

[2] A visit is a sequence of successive CHEOPS orbits devoted to observing a given target.

radius is automatically set based on the signal-to-noise ratio (S/N). In addition to the subarrays, there are imagettes available for each exposure. The imagettes are frames of 30 pixels in radius centred on the target, which do not need to be co-added before download owing to their smaller size. We used a tool specifically developed for photometric extraction of imagettes using point-spread function photometry, called PIPE[3]; see for example Szabó et al. (2021, 2022). The PIPE photometry has a S/N comparable to that of DRP photometry, but has the advantage of shorter cadence, and therefore we decided to use this CHEOPS product in this work. The average uncertainty of the PIPE data points is 160 ppm.

The PIPE CHEOPS observations were processed using the dedicated data decorrelation and transit analysis software called pycheops[4] (Maxted et al. 2022). This package includes downloading, visualising, and decorrelating CHEOPS data, fitting transits and eclipses of exoplanets, and calculating light-curve noise. We first cleaned the light curves from outlier data points using the pycheops built-in function clip_outliers, which removes outliers from a dataset by calculating the mean absolute deviation (MAD) from the light curve following median smoothing, and rejects data greater than the smoothed dataset plus the MAD multiplied by a clipping factor. The clipping factor equal to five was reasonable in our cases, which we checked visually. With this clipping procedure, we discarded 30 data points out of 3195, which is ~0.9% of the CHEOPS data. The next step was the extraction of the detrending parameters. During this procedure, the software gives a list of the parameters necessary for the detrending. The most important decorrelation is subtraction of the roll-angle effect. In order to keep the cold plate radiators facing away from the Earth, the spacecraft rolls during its orbit. This means that the field of view rotates around the pointing direction. The target star remains stationary within typically 1 pixel, but the rotation of the field of view produces a variation of its flux from the nearby sources in phase with the roll angle of the spacecraft (Bonfanti et al. 2021). The extracted detrending parameters were co-fitted with the transit model (see Sect. 3.3).

2.3. ESPRESSO/VLT data

We acquired 14 high-resolution spectra of the host star HD 22946 using the ESPRESSO spectrograph (Pepe et al. 2014) mounted at the 8.2 m Very Large Telescope (VLT) at Paranal Observatory (Chile). The observations were carried out between 10 February 2019 and 17 March 2019 under the observing program number 0102.C-0456 (PI: V. Van Eylen) and within the KESPRINT[5] project. We used the high-resolution (HR) mode of the spectrograph, which provides a resolving power of $R \approx 134\,000$. We set the exposure time to 600 s, leading to a S/N per pixel at 650 nm ranging between 120 and 243. Daytime ThAr spectra and simultaneous Fabry-Perot exposures were taken to determine the wavelength solution and correct for possible nightly instrumental drifts, respectively. We reduced the ESPRESSO spectra using the dedicated data-reduction software and extracted the RVs by cross-correlating the échelle spectra with a G2 numerical mask. We list the ESPRESSO RV measurements in Table 3. The average uncertainty of the RV data points is ~0.00015 km s^{-1}.

We co-added the individual ESPRESSO spectra prior to carrying out the spectroscopic analysis presented in Sect. 3.1. To this aim, we Doppler-shifted the data to a common reference wavelength by cross-correlating the ESPRESSO spectra

Table 3. Log of ESPRESSO/VLT RV observations of HD 22946.

Time (BJD$_{TDB}$)	RV value (km s^{-1})	$\pm 1\sigma$ (km s^{-1})
2458524.56069831	16.85125	0.00011
2458525.55490396	16.85217	0.00013
2458526.59541816	16.85512	0.00011
2458527.63233315	16.85284	0.00022
2458535.62345024	16.84839	0.00036
2458540.53620531	16.85020	0.00010
2458550.57174504	16.85549	0.00020
2458552.56783808	16.85330	0.00016
2458553.51738686	16.86251	0.00011
2458556.50131285	16.85536	0.00014
2458557.50492574	16.85738	0.00009
2458557.56483059	16.85716	0.00010
2458558.52709593	16.85741	0.00010
2458559.54006749	16.85690	0.00016

with the spectrum with the highest S/N. We finally performed a S/N-weighted co-addition of the Doppler-shifted spectra, while applying a sigma-clipping algorithm to remove possible cosmic-ray hits and outliers. The co-added spectrum has a S/N of ~900 per pixel at 650 nm.

3. Data analysis and first results

3.1. Stellar parameters

The spectroscopic stellar parameters (the effective temperature $T_{\rm eff}$, the surface gravity $\log g$, the microturbulent velocity $v_{\rm mic}$, and the metallicity [Fe/H]; see Table 4) were derived using the ARES and MOOG codes, following the same methodology as described in Santos et al. (2013), Sousa (2014), and Sousa et al. (2021). We used the latest version of the ARES code[6] (Sousa et al. 2007, 2015) to measure the equivalent widths of iron lines on the combined ESPRESSO spectrum. We used a minimisation procedure to find ionisation and excitation equilibrium and converge to the best set of spectroscopic parameters. This procedure makes use of a grid of Kurucz model atmospheres (Kurucz 1993a) and the radiative transfer code MOOG (Sneden 1973).

To derive the radius of the host star HD 22946, we used a Markov-Chain Monte Carlo (MCMC) modified infrared flux method. This enables us to calculate the bolometric flux using stellar atmospheric models defined by our spectral analysis to build spectral energy distributions (SEDs) that are compared with broadband fluxes and uncertainties from the most recent data releases for the following bandpasses: *Gaia G*, $G_{\rm BP}$, and $G_{\rm RP}$, 2MASS *J*, *H*, and *K*, and WISE W1 and W2 (Skrutskie et al. 2006; Wright et al. 2010; Gaia Collaboration 2021). From the bolometric flux, we then determine stellar effective temperature and angular diameter; this latter is converted to a radius using the offset-corrected *Gaia* parallax (Lindegren et al. 2021). We used Bayesian modeling averaging of the ATLAS (Kurucz 1993b; Castelli & Kurucz 2003) and PHOENIX (Allard 2014) catalogues to produce a weighted averaged posterior distribution of the stellar radius in order to account for uncertainties in stellar atmospheric modelling. We find a value of $R_{\rm s} = 1.117 \pm 0.009\,R_\odot$, which is in 3σ agreement with the value of $1.157 \pm 0.025\,R_\odot$ presented by the discoverers.

We finally determined the stellar mass $M_{\rm s}$ and stellar age $t_{\rm s}$ using two different sets of stellar evolutionary models,

---

[3] See https://github.com/alphapsa/PIPE
[4] See https://github.com/pmaxted/pycheops
[5] See https://kesprint.science/

[6] The last version, ARES v2, can be downloaded at https://github.com/sousasag/ARES

Table 4. Fundamental parameters of the exoplanet host HD 22946.

Parameter (unit)	Value	Source
Name	HD 22946	–
TOI ID	411	G2021
TIC ID	100990000	S2018
Gaia DR3 ID	4848767461548943104	G2022
RA (J2016) (deg)	54.819528	G2022
Dec (J2016) (deg)	−42.76304	G2022
T (TESS) (mag)	7.757 ± 0.006	S2018
G (*Gaia*) (mag)	8.13 ± 0.69	G2022
J (mag)	7.250 ± 0.027	C2003
H (mag)	7.040 ± 0.044	C2003
K (mag)	6.981 ± 0.029	C2003
$T_{\rm eff}$ (K)	6040 ± 48	C2022
$T_{\rm eff}$ (K)	6169 ± 64	This work
$R_{\rm s}$ ($R_\odot$)	1.157 ± 0.025	C2022
$R_{\rm s}$ ($R_\odot$)	1.117 ± 0.009	This work
$M_{\rm s}$ ($M_\odot$)	1.104 ± 0.012	C2022
$M_{\rm s}$ ($M_\odot$)	$1.098^{+0.040}_{-0.039}$	This work
$\log g$ (cgs)	4.26 ± 0.15	C2022
$\log g$ (cgs)	4.47 ± 0.11	This work
[Fe/H] (dex)	−0.14 ± 0.07	C2022
[Fe/H] (dex)	−0.08 ± 0.04	This work
$t_{\rm s}$ (Gyr)	5.0 ± 1.0	C2022
$t_{\rm s}$ (Gyr)	2.5 ± 1.0	This work
$v_{\rm mic}$ (km s^{-1})	1.25 ± 0.03	This work

Notes. Abbreviations refer to the following sources: G2021 = Guerrero et al. (2021), S2018 = Stassun et al. (2018), G2022 = Gaia Collaboration (2023), C2003 = Cutri et al. (2003), C2022 = Cacciapuoti et al. (2022).

namely PARSEC[7] v1.2S (Marigo et al. 2017) and CLES (Code Liègeois d'Évolution Stellaire), see Scuflaire et al. (2008). More specifically, we employed the isochrone-placement algorithm developed by Bonfanti et al. (2015, 2016) to interpolate the input parameters ($T_{\rm eff}$, [Fe/H], $R_{\rm s}$) within pre-computed grids of PAR-SEC v1.2S isochrones and tracks to derive a first pair of mass and age. A second pair of mass and age values, instead, was retrieved by inputting $T_{\rm eff}$, [Fe/H], and $R_{\rm s}$ directly in the CLES code, which generates the best-fit stellar evolutionary track following the Levenberg-Marquadt minimisation scheme, as described in Salmon et al. (2021). After carefully checking the mutual consistency of the two respective pairs of outcomes through the χ^2-based methodology presented in Bonfanti et al. (2021), we finally merged (i.e. summed) the two $M_{\rm s}$ and $t_{\rm s}$ results and obtained $M_{\rm s} = 1.098 \pm 0.040\ M_\odot$ and $t_{\rm s} = 2.5 \pm 1.0$ Gyr. The mass parameter value of the host star agrees within the uncertainty with the value provided in the discovery paper, which is $1.104 \pm 0.012\ M_\odot$. However, the planet host seems to be younger than previously presented by C22. The discoverers obtained a value of 5.0 ± 1.0 Gyr. More parameter values, including from this work, are compared with the discovery-paper parameter values in Table 4.

3.2. Period aliases of HD 22946d from the TESS data

In order to determine each possible period alias and to schedule CHEOPS observations of planet d, we first performed a period analysis of the available TESS data. For this purpose, we used

Table 5. Orbital period aliases of the planet HD 22946d.

Alias No.	Period alias (P) (days)	Probability (p) (%)
1	39.5206	17.420
2	41.8454	20.078
3	44.4607	20.341
4	47.4248	18.113
5	50.8122	13.445
6	54.7209	7.061
7	59.2809	2.756
8	64.6701	~1.0

Notes. Only the period aliases with a probability of $p > 1\%$ are listed here, as calculated by the `MonoTools` package from TESS data alone, i.e. before CHEOPS observations.

the `MonoTools` package[8] (Osborn et al. 2022), which is able to model transit light curves in case of multiple transits, duotransits, and monotransits, as well as multiple systems with combinations of such candidates, with both radial velocities and transit photometry. The package calculates a marginalised probability distribution across all allowed aliases for a given transit model by combining priors for each alias. The probabilities are estimated based on two major assumptions, namely that short-period orbits are highly favoured over long-period ones due to a combination of geometric probability and window function, and that planets in multi-planet systems have low eccentricities (Kipping et al. 2013; Van Eylen & Albrecht 2015; Kipping 2018). More details about this software can be found in Osborn et al. (2022).

The TESS data described in Sect. 2.1 were used during the fitting procedure using `MonoTools`. In the case of planet b, we set as input parameters the reference mid-transit time of $T_{\rm c} = 2\,458\,385.7318$ BJD$_{\rm TDB}$, the orbital period of $P_{\rm orb} = 4.040330 \pm 0.000010$ days, the transit duration (transit width) of $W = 3.4$ h, and the transit depth of $D = 134$ ppm. In the case of planet c, the inputs were $T_{\rm c} = 2\,458\,386.1878$ BJD$_{\rm TDB}$, $P_{\rm orb} = 9.573117 \pm 0.000020$ days, $W = 3.8$ h, and $D = 389$ ppm. For planet d, we set as input parameters the two mid-transit times detected by TESS, namely $t_{\rm tr,1} = 2\,458\,425.1657$ BJD$_{\rm TDB}$ and $t_{\rm tr,2} = 2\,459\,136.5357$ BJD$_{\rm TDB}$, the transit duration of $W = 6.5$ h and the transit depth of $D = 478$ ppm. These parameters were calculated from the TESS data alone.

The orbital period aliases of planet d with a probability of $p > 1\%$ are listed in Table 5. The software `MonoTools` forecasted that a transit of planet d with the orbital period alias number 2 would take place on 25 October 2021, with a mid-transit time of $T_{\rm c} = 2\,459\,513.1441$ BJD$_{\rm TDB}$. This forecasted event was observed during the third CHEOPS visit (see Table 2), but the expected transit of planet d did not happen; only the transit of planet b was recorded that time. After this observation, we were able to exclude the period alias of $P = 41.8454$ days from the list of possible aliases. The next forecast predicted a transit of planet d on 28 October 2021, with a mid-transit time of $T_{\rm c} = 2\,459\,515.9338$ BJD$_{\rm TDB}$, which means that, in this case, the alias number 4 (see Table 5) was preferred as its true orbital period. This forecasted event was observed with CHEOPS during its fourth visit. This time, the transit of planet d was successfully detected together with a transit of planet c, confirming that the period alias of $P = 47.4248$ days is the true orbital period of planet d. This result also confirms that the

second transit-like feature of planet d, observed by TESS in sector number 30, was a real transit event and not an instrumental artifact as considered by C22. Alternatively, the dip observed at 2 459 136.5357 BJD$_{TDB}$ was a mixture of instrumental effects and the transit of planet d. With this gathered knowledge about the true orbital period of planet d, we were able to combine CHEOPS and TESS photometric observations and RV measurements in order to improve the orbital and planetary parameters of the HD 22946 system, which were previously obtained only from the TESS and RV data by the discoverers.

3.3. CHEOPS, TESS, and RV combined model

In order to produce accurate planetary parameters for all three planets, we built a combined model using all available data, that is, TESS photometry (described in Sect. 2.1), CHEOPS photometry (described in Sect. 2.2), and ESPRESSO RVs (described in Sect. 2.3). The combined model was built using the `PyMC3` package[9] (Salvatier et al. 2016), which performs Hamiltonian Monte Carlo (HMC) sampling, with Keplerian orbits modeled with `exoplanet` package[10] (Foreman-Mackey et al. 2021). We used Gaussian processes (GPs) to model the stellar variability present in the TESS light curve, opting for a simple harmonic oscillator (SHO) kernel implemented in the `celerite` package (Foreman-Mackey et al. 2017) and a quality factor $Q = 1/\sqrt{2}$, as is common for quasi-periodic stellar variability. In order to speed up sampling, we binned the TESS data to 30 min bins far from transits, keeping 2 min data near transit. As we have reasonable prior knowledge from theoretical analyses for the expected stellar limb-darkening (LD) parameters for HD 22946, we used these as priors in the analysis. We used the quadratic LD law and interpolated tables of coefficients calculated for the TESS (Claret 2018) and CHEOPS (Claret 2021) passbands using the derived stellar parameters of T_{eff} = 6169 K and $\log g$ = 4.47 (cgs). In order to guard against systematic errors, we inflated the σ for each parameter prior to 0.1.

Even though the `PIPE` light curves for HD 22946 have fewer systematic features than the DRP light curves, they can still include flux variations due to the influence of various external factors. Therefore, we can improve the light curve by decorrelating the flux data against metadata generated for the instrument and target. To decipher which decorrelation vectors provide improvement, we ran an initial `PyMC3` model for each CHEOPS visit using all available ancillary data – sin and cos of roll-langle, background flux, x and y centroid positions, onboard temperature and time (which also fits short-timescale stellar variability). These parameters are normalised to have $\mu = 0.0$ and $\sigma = 1.0$, and decorrelation parameters are given normal priors with $\mu = 0.0$ and σ set by the root-mean-square (RMS) noise for each CHEOPS visit. For each visit model, we also included parameters for any planetary transits present in order to ensure the transits would not bias the model. After HMC sampling, we assessed each decorrelation parameter using the average and standard deviations, keeping only those parameters with a Bayes Factor of BF > 1. Despite this detrending, shorter-timescale variation can also be present as a function of roll angle (φ). Pure detrending against sin and cos of roll angle removes the largest amplitude systematic trends at low frequencies. These are those closest in timescale to the transit feature, and so a simpler detrending technique for such timescales guards against overfitting of the transit. However, the CHEOPS light curve typically

also contains systematic noise correlated with roll angle that is at a lower amplitude and higher frequency. This is not therefore adequately removed by simple sin and cos decorrelation. It is this noise that a more flexible GP is better able to model. We therefore also included a GP to model the variation of flux with roll-angle effects. To do this, we first found any potential large jumps in φ and made sure the time series was continuous between these jumps (i.e. by moving the zero point and 'wrapping around'). We then transformed the input data such that it is continuous in x – by sorting by φ rather than time. Once again, we used a SHO kernel from `celerite` with quality factor Q set at $1/\sqrt{2}$. As we expected the morphology of the variations to be preserved for all CHEOPS visits, we used a single shared kernel. We found that the linear decorrelation is the most important, decreasing the log likelihood by a factor of 1400, but the GP is responsible for a reduction of a further 450, which means that use of a GP to model roll-angle flux behaviour is well justified.

As multi-planet systems typically have low eccentricities e (Van Eylen et al. 2019), and we lack the high number of RVs capable of resolving any differences in e, we chose to fit only circular orbits. In order to guard against unphysical negative values, we used broad log-normal priors for the key transit and RV amplitude parameters, that is, for R_p/R_s (planet-to-star radius ratio) and K (RV semi-amplitude). The quantities derived in Sect. 3.1 are used as priors on the stellar parameters in the model. For all datasets – CHEOPS, TESS, and ESPRESSO –, we included a jitter term using a wide log-normal prior. We then sampled the combined model using the `PyMC_ext` 'sample' function, which is specifically written for astrophysical applications, and allows us to group independent dataset parameters (e.g. the CHEOPS visit-specific decorrelation parameters) together, thereby speeding up sampling greatly. We used ten chains, tuning each for 1300 steps before sampling for a further 1800, resulting in 18 000 unique samples. The sample have effective sample sizes in the thousands, and the gelmin-rubin statistics are below 1.01 for all parameters, suggesting they are sufficiently uncorrelated and unbiased. The full list of fitted GP hyperparameters and detrending parameters with the corresponding best-fitting values can be found in Appendix A.1. The best-fitting and derived parameters of the system are described and discussed in Sect. 4.

3.4. Search for transit-timing variations

In order to look for potential TTVs, we also ran a combined model using unconstrained timing for each planetary transit thanks to the `TTVorbit` function of `exoplanet`, and an independent analysis using the `Allesfitter` software[11] (Günther & Daylan 2019, 2021), applying a nested sampling fit. Although C22 already performed such an analysis and found no obvious sign of TTVs in the system, we repeated this procedure, but in this case using the CHEOPS data as well. This means mainly that we included three transits of planet d in the analysis and used a longer time baseline. We used the same dataset as in Sect. 3.3, which was co-fitted with a GP using the `celerite SHO` kernel in both cases. All planetary and system parameters were fixed as derived previously, only the GP hyperparameters, the detrending parameters, and the observed-minus-calculated (O-C) parameters for individual mid-transit times were fitted. Both solutions are consistent with a linear ephemeris, which means we did not find any indication of a quadratic trend in the data, in agreement with the conclusion made by the discoverers. As an illustration,

---

[9] See https://pypi.org/project/pymc3/
[10] See https://pypi.org/project/exoplanet/

[11] See https://www.allesfitter.com/

Table 6. Best-fitting and derived system and planetary parameters of the HD 22946 planetary system.

Parameter (unit)	Description	HD 22946b	HD 22946c	HD 22946d
T_c (BJD$_{TDB}$)	Reference mid-transit time	$2\,458\,385.7321^{+0.0022}_{-0.0031}$	$2\,459\,161.60861^{+0.00069}_{-0.00072}$	$2\,459\,136.53720^{+0.00087}_{-0.00083}$
P_{orb} (days)	Orbital period	$4.040295^{+0.000015}_{-0.000014}$	9.573083 ± 0.000014	$47.42489^{+0.00010}_{-0.00011}$
b	Impact parameter	$0.21^{+0.11}_{-0.13}$	$0.504^{+0.024}_{-0.026}$	$0.456^{+0.026}_{-0.028}$
a/R_s	Scaled semi-major axis	11.03 ± 0.12	$19.61^{+0.22}_{-0.23}$	57.00 ± 0.66
a (au)	Semi-major axis	$0.05727^{+0.00085}_{-0.00082}$	$0.1017^{+0.0015}_{-0.0014}$	$0.2958^{+0.0044}_{-0.0042}$
R_p/R_s	Planet-to-star radius ratio	$0.01119^{+0.00031}_{-0.00032}$	$0.01912^{+0.00026}_{-0.00027}$	$0.02141^{+0.00046}_{-0.00045}$
t_{dur} (days)	Transit duration	$0.1281^{+0.0026}_{-0.0037}$	$0.1535^{+0.0015}_{-0.0014}$	$0.2701^{+0.0019}_{-0.0020}$
R_p ($R_\oplus$)	planet radius	1.362 ± 0.040	$2.328^{+0.038}_{-0.039}$	2.607 ± 0.060
M_p ($M_\oplus$)	planet mass[*]	13.71	9.72	26.57
$M_{p,est}$ ($M_\oplus$)	Estimated planet mass[♣]	2.42 ± 0.12	6.04 ± 0.17	7.32 ± 0.28
$M_{p,est}$ ($M_\oplus$)	Estimated planet mass[♡]	2.61 ± 0.27[†]	6.61 ± 0.17[‡]	7.90 ± 0.28[‡]
ρ_p (g cm^{-3})	planet density[*]	18.96	3.15	10.80
K (m s^{-1})	RV semi-amplitude[*]	5.05	2.70	4.31
I_p (W m^{-2})	Insolation flux	$673\,884^{+32\,444}_{-31\,606}$	$213\,337^{+10\,270}_{-10\,006}$	$25\,261^{+1216}_{-1184}$
T_{surf} (K)	Surface temperature[◇]	1241 ± 14	931 ± 11	546 ± 6
TSM	Transmission spectroscopy metric[♯]	43 ± 4	63 ± 2	43 ± 2

Notes. Based on the joint fit of the TESS and CHEOPS photometric data and RV observations. Table shows the best-fitting value of the given parameter and its $\pm 1\sigma$ uncertainty. The fitted values correspond to quantile 0.50 (median) and the uncertainties to quantils ± 0.341 in the parameter distributions obtained from the samples. [*]Only the 3σ upper limits are listed here due to the low number of the RV observations. [◇]Assuming the albedo value of 0.2. [♣]Based on the relations presented by Chen & Kipping (2017), assuming that the planet radii are from the interval of $1.23 < R_p < 14.26\ R_\oplus$. [♡]Based on the relations presented by Otegi et al. (2020). [†]Assuming that $\rho_p > 3.3$ g cm^{-3}. [‡]Assuming that $\rho_p < 3.3$ g cm^{-3}. [♯]Based on the criteria set by Kempton et al. (2018), using the scale factor of 1.26, the stellar radius of $R_s = 1.117 \pm 0.009\ R_\odot$ and $J = 7.250 \pm 0.027$ mag (see Table 4).
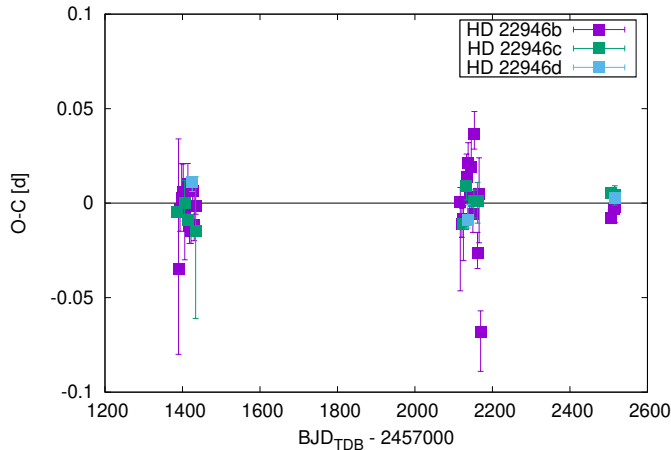

Fig. 1. Observed-minus-calculated (O-C) diagram of mid-transit times of the planets HD 22946b, HD 22946c, and HD 22946d obtained using the `Allesfitter` package. The O-C values are consistent with a linear ephemeris, which means no significant TTVs are present in the system.

the obtained O–C diagram of the mid-transit times for planets b, c, and d from the `Allesfitter` package is depicted in Fig. 1. We can see that the O–C values are scattered around O–C = 0.0 d, which means that no significant TTVs are present in the system.

4. Final results and discussion

The best-fitting and derived parameters from the combined model are listed in Table 6, and the model posteriors of the host star are summarised in Appendix A.2. The fitted TESS light curves from sector numbers 3, 4, 30, and 31 are depicted in the panels of Figs. 2 and 3. The CHEOPS individual observations

overplotted with the best-fitting models are shown in the panels of Fig. 4. The RV observations fitted with a spectroscopic orbit are depicted in Fig. 5.

Here, we present new ephemerides of the planetary orbits, which we calculated based on the combined model. Thanks to the combined TESS and CHEOPS observations, we were able to improve the reference mid-transit times and the orbital periods of the planets compared to the discovery values. C22 derived the orbital period parameter values of $P_{orb,b} = 4.040301^{+0.000023}_{-0.000042}$ days and $P_{orb,c} = 9.573096^{+0.000026}_{-0.000023}$ days, and expected an orbital period of $P_{orb} = 46 \pm 4$ days for planet d, which was estimated based on the transit duration and depth along with stellar mass and radius through *Kepler*'s third law, assuming circular orbits. We confirmed this prediction, finding an orbital period for planet d of $P_{orb} = 47.42489 \pm 0.00011$ days. The improved ratios of the orbital periods are $P_{orb,c}/P_{orb,b} = 2.37$ and $P_{orb,d}/P_{orb,c} = 4.95$. Based on the *Kepler* database, the adjacent planet pairs in multiple systems show a broad overall peak between period ratios of 1.5 and 2, followed by a declining tail to larger period ratios. In addition, there appears to be a sizeable peak just interior to the period ratio 5 (Steffen & Hwang 2015); therefore, we can say that the period ratios in HD 22946 fall into statistics and the seemingly large orbital gap between planets c and d is not anomalous.

In the combined model, we determined the impact parameter b, which is the projected relative distance of the planet from the stellar disk centre during the transit midpoint in units of R_s. Converting these parameter values to the orbit inclination angle values we can obtain $i = 88.90^{+0.16}_{-0.05}$ deg, $i = 88.52^{+0.08}_{-0.07}$ deg, and $i = 89.54^{+0.02}_{-0.03}$ deg for planets b, c, and d, respectively. For comparison, we note that the corresponding discovery values are $i_b = 88.3^{+1.1}_{-1.2}$ deg and $i_c = 88.57^{+0.86}_{-0.53}$ deg. The inclination
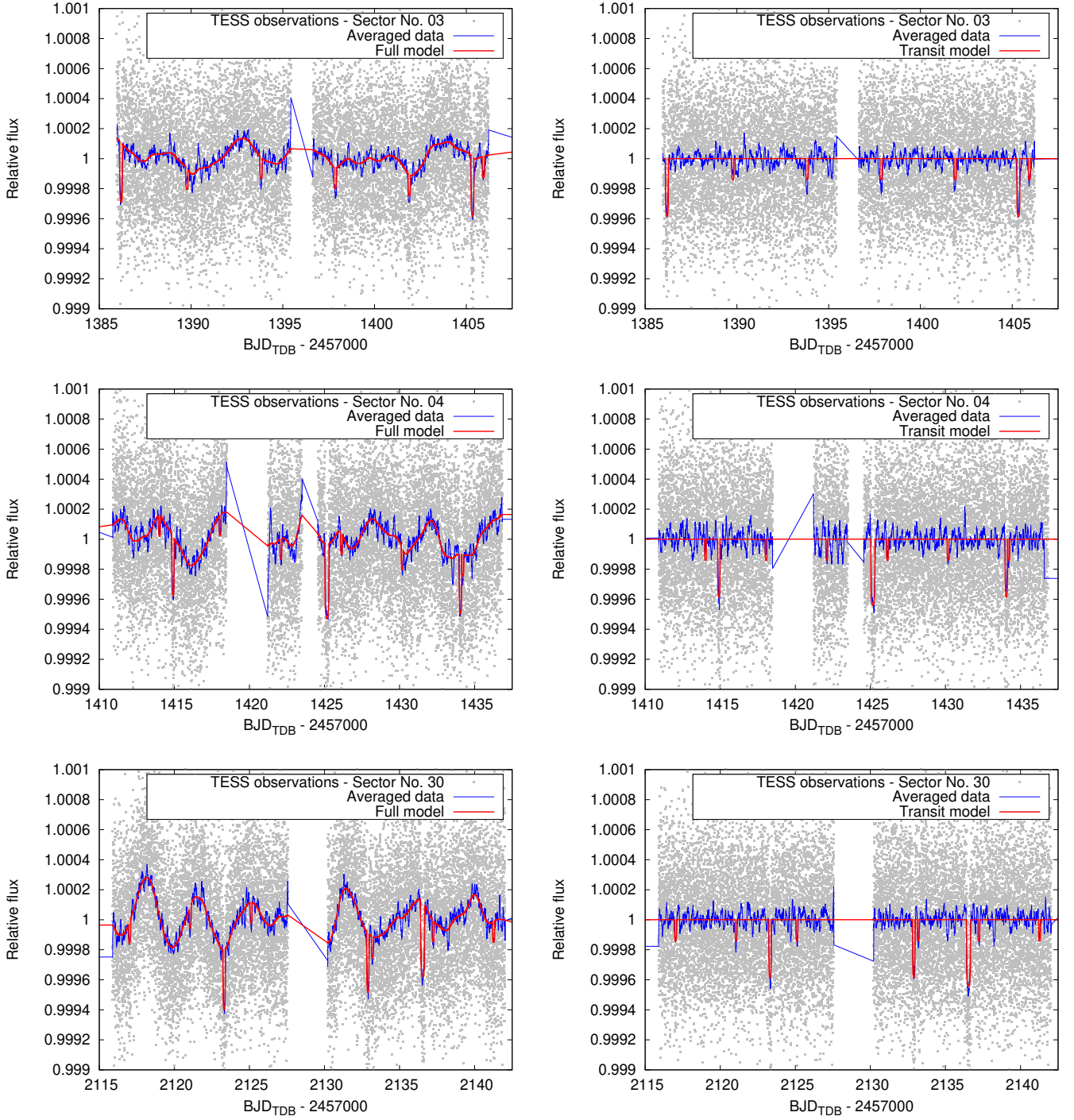
Fig. 2. TESS observations of the transiting planets HD 22946b, HD 22946c, and HD 22946d from sector numbers 3, 4, and 30 overplotted with the best-fitting model. This model was derived based on the entire CHEOPS and TESS photometric dataset and the RV observations from ESPRESSO via joint analysis of the data. The left-hand panels show the non-detrended data overplotted with the full model, while the right-hand panels show the detrended data overplotted with the transit model. We averaged the TESS data for better visualisation of the transit events using a running average with steps and width of 0.009 and 0.09 day, respectively. We note that an interruption in communications between the instrument and spacecraft occurred at 2 458 418.54 BJD_{TDB}, resulting in an instrument turn-off until 2 458 421.21 BJD_{TDB}. No data were collected during this period.

angle of planet d was not determined by C22. According to the improved parameter values, it seems that only the orbits of planets b and c are well aligned. planet d is probably not in the same plane as planets b and c.

Based on the combined TESS and CHEOPS photometry observations, we redetermined the radii of the planets, which are $1.362 \pm 0.040\ R_{\oplus}$, $2.328 \pm 0.039\ R_{\oplus}$, and $2.607 \pm 0.060\ R_{\oplus}$

for planets b, c, and d, respectively. The CHEOPS observations are an added value, because compared to the corresponding parameter values presented in C22 ($R_{p,b} = 1.72 \pm 0.10\ R_{\oplus}$, $R_{p,c} = 2.74 \pm 0.14\ R_{\oplus}$, and $R_{p,d} = 3.23 \pm 0.19\ R_{\oplus}$), there is a noticeable improvement in radius precision. Using TESS and CHEOPS photometry observations, the uncertainties on the planet radius parameter values were decreased by ~50%, 68%, and 61% for
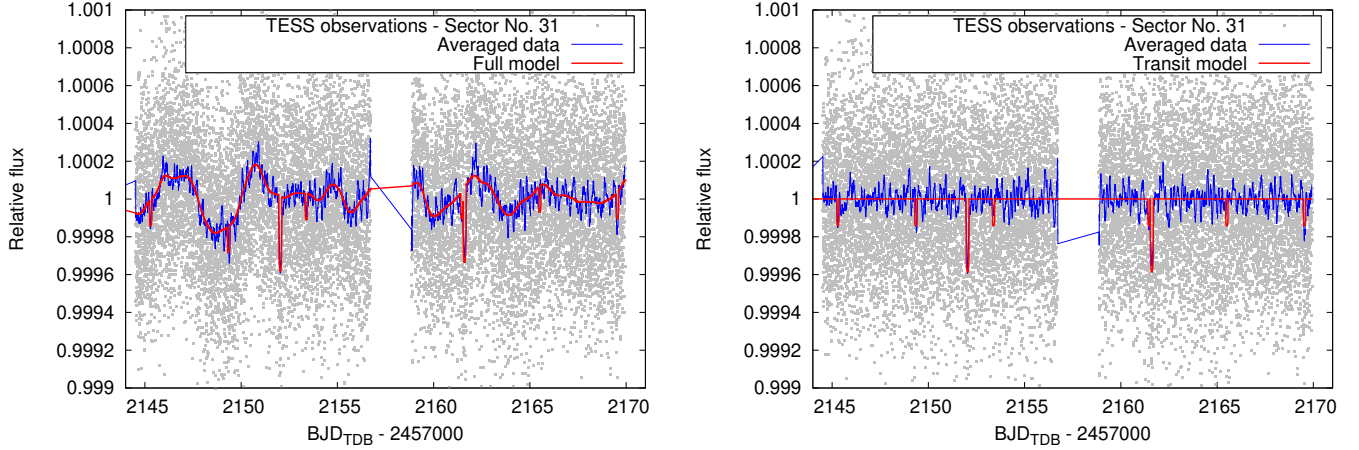
Fig. 3. As in Fig. 2, but for the TESS sector number 31.

planets b, c, and d, respectively. We also note that the parameter values from this work are in stark contrast to those derived by C22; these authors found significantly larger radii, that is, larger by ~21%, 15%, and 19% for planets b, c, and d, respectively. We believe this may be due to a misunderstanding of the `LimbDarkLightCurve` function in `exoplanet`. The function requires the planetary radius R_p in solar radii rather than the planet-to-star radius ratio R_p/R_s. When misused, the result is an inflation of R_p/R_s and R_p values by a factor of $R_s/R_\oplus$, which in this case is a factor of about 15%–21%. This mistake can be seen most clearly in C22, when comparing the models shown in Fig. 5 with the implied depths in Table 4 (likely derived from the radius ratio), which are inflated by this factor. Such a mistake was also evident during the reanalysis of the BD+40 2790 (TOI-2076) system (Osborn et al. 2022).

According to the radius valley at ~1.5–2.0 $R_\oplus$, which separates super-Earths and sub-Neptunes (Fulton et al. 2017; Van Eylen et al. 2018; Martinez et al. 2019; Ho & Van Eylen 2023), and based on the refined planet radii, we find that planet b is a super-Earth, and planets c and d are similar in size and are sub-Neptunes, in agreement with C22. It is well known that small exoplanets have bimodal radius distribution separated by the radius valley. Potential explanations focus on atmospheric-escape-driven mechanisms, such as photoevaporation; see for example Owen (2019). The models showed that those planets that have radius below 1.5 $R_\oplus$ were planets that initially had hydrogen/helium atmospheres, but ultimately lost them due to atmospheric escape, while those just above 2.0 $R_\oplus$ had hydrogen/helium atmosphere masses of ~1% of the core mass. Having HD 22946 planets on either side of the valley means that planet b could be a photo-evaporated version of planets c and d. Recently, Luque & Pallé (2022) presented a brand new approach, arguing that the density of planets might provide more information than planet radii alone and proposing that a density gap separates rocky from waterrich planets. For M dwarf systems, these authors found that rocky planets form within the ice line while water worlds formed beyond the ice line and migrated inwards. Given that theoretical models predict similar results for stars of other types, this scenario could also be possible in the case of the planets orbiting HD 22946.

Due to the low number of RVs, here we present only the 3σ upper limits for the planet masses in agreement with the discoverers. C22 obtained the 3σ upper mass limits of about 11 $M_\oplus$, 14.5 $M_\oplus$, and 24.5 $M_\oplus$ for planets b, c, and d,

respectively, from the same spectroscopic observations. The 3σ upper limits for the planet masses from this work are $M_{p,b} = 13.71\ M_\oplus$, $M_{p,c} = 9.72\ M_\oplus$, and $M_{p,d} = 26.57\ M_\oplus$. Similarly to the discoverers, we obtained very different upper mass limits for planets c and d, although they have similar planet radii, which could be due to a somewhat different internal structure of these planets. Applying the relations of Chen & Kipping (2017) and Otegi et al. (2020), we also re-estimated the planet masses, which were previously forecasted by the discoverers as $6.29 \pm 1.30\ M_\oplus$, $7.96 \pm 0.69\ M_\oplus$, and $10.53 \pm 1.05\ M_\oplus$ for planets b, c, and d, respectively. The improved parameter values are presented in Table 6. Furthermore, taking into account the estimated planet masses calculated based on the relations of Otegi et al. (2020), we predicted the number of additional RV measurements required to achieve a 3σ detection on each mass using the `Radial Velocity Follow-up Calculator`[12] (RVFC; see Cloutier et al. 2018), and the `RV simulator` (Wilson et al., in prep.). Based on these simulations, we obtained that another 27, 24, and 48 ESPRESSO RVs are needed to measure the predicted masses of planets b, c, and d, respectively. The expected RV semi-amplitudes assuming the estimated planet masses are $K_b = 1.10 \pm 0.12\ m\ s^{-1}$, $K_c = 2.08 \pm 0.10\ m\ s^{-1}$, and $K_d = 1.46 \pm 0.08\ m\ s^{-1}$.

C22 also probed the planets from the viewpoint of future atmospheric characterisation using the transmission spectroscopy metric (TSM); see Eq. (1) in Kempton et al. (2018). The authors obtained the TSM values of 65 ± 10, 89 ± 16, and 67 ± 14 for planets b, c, and d, respectively. We revised these values based on the results from the present work. The improved TSM values (see Table 6) do not satisfy the recommended value of TSM > 90 for planets with a radius of $1.5 < R_p < 10\ R_\oplus$. On the other hand, given that this threshold is set very rigorously, in agreement with the discoverers, we can note that planet c could be a feasible target for transmission spectroscopy observations with future atmospheric characterisation missions, such as the planned *Ariel* space observatory (Tinetti et al. 2021).

Finally, we discuss the relevance of planet d among the known population of similar exoplanets. HD 22946d represents a warm sub-Neptune. Based on the NASA Exoplanet Archive[13] (Akeson et al. 2013), there are 5272 confirmed exoplanets up to 22 February 2023, but only 63 planets out of 5272 are

---

[12] See http://maestria.astro.umontreal.ca/rvfc/
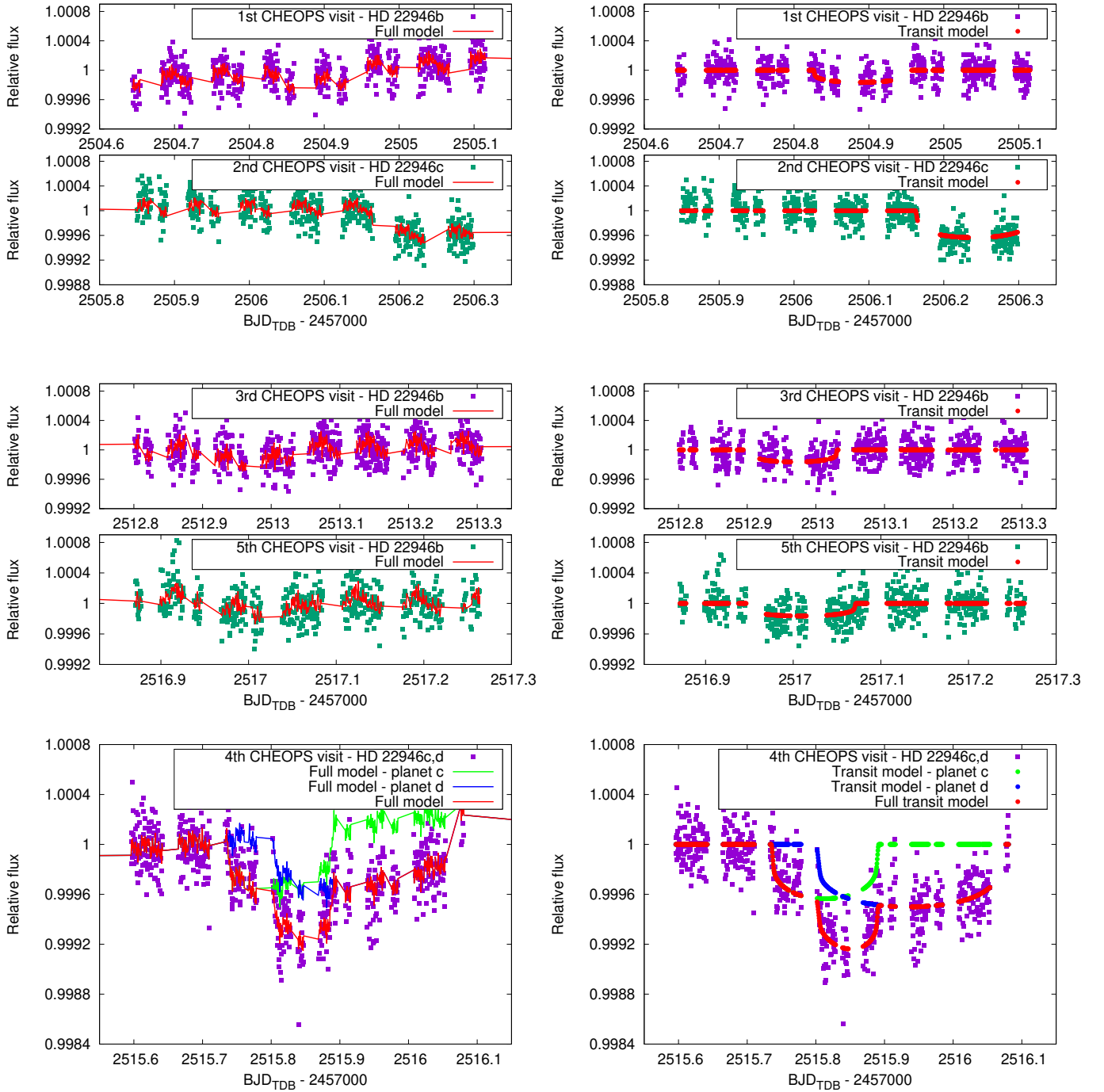[13] See https://exoplanetarchive.ipac.caltech.edu/index.html

Fig. 4. Individual CHEOPS observations of the transiting planets HD 22946b, HD 22946c, and HD 22946d. The observed light curves are overplotted with the best-fitting model. This model was derived based on the entire CHEOPS and TESS photometric dataset and the RV observations from ESPRESSO via joint analysis of the data. The left-hand panels show the non-detrended data overplotted with the full model, while the right-hand panels show the detrended data overplotted with the transit model. In the case of the fourth CHEOPS visit, as the multiple transit feature, the individual transit models of planets c and d are also shown in addition to the summed model.

sub-Neptune sized ($1.75 < R_p < 3.5 \, R_\oplus$) and transiting bright stars ($G \leq 10$ mag). Only 7 planets out of 63 have orbital periods longer than 30 days and only 4 planets out of 7 have an equilibrium temperature of below 550 K. Three planets have a lower insolation flux than planet d, namely TOI-2076d (Osborn et al. 2022), HD 28109d (Dransfield et al. 2022), and HD 191939 (Badenas-Agusti et al. 2020). HD 22946d is therefore an interesting target for future follow-up observations. One

of the questions to be answered in the near future is the composition and internal structure of sub-Neptune-type planets. Using CHEOPS observations, we determined the radius of planet d with high accuracy. Its true mass could be determined with another 48 ESPRESSO RV measurements according to the estimate we present above. A combination of mass and radius gives the overall density, which will be an important step forward towards understanding sub-Neptunes.
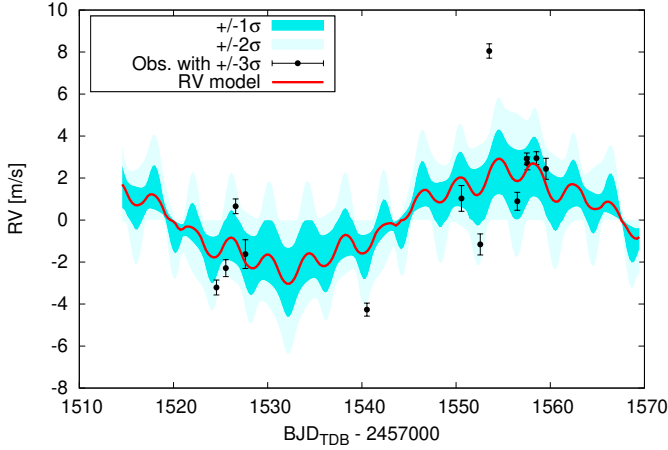
Fig. 5. RV observations taken at ESPRESSO fitted with a spectroscopic orbit (red line). The 1σ and 2σ uncertainties of the model are plotted as coloured areas. The uncertainties of the individual RV data points correspond to a 3σ interval.

5. Conclusions

Based on the combined TESS and CHEOPS observations, we refined several parameters of the HD 22946 planetary system. First of all, we improved the ephemerides of the planetary orbits in comparison with the discovery values. We can confirm that planets b and c have short orbital periods below 10 days, namely 4.040295 ± 0.000015 days and 9.573083 ± 0.000014 days, respectively. The third planet, HD 22946d, has an orbital period of 47.42489 ± 0.00011 days, which we were able to derive based on additional CHEOPS observations. Furthermore, based on the combined TESS and CHEOPS observations, we derived precise radii for the planets, which are $1.362 \pm 0.040\ R_\oplus$, $2.328 \pm 0.039\ R_\oplus$, and $2.607 \pm 0.060\ R_\oplus$ for planets b, c, and d, respectively. On the one hand, we can confirm the conclusion of the discoverers that the planetary system consists of a super-Earth, and planets c and d are sub-Neptunes. On the other hand, we find the planet radii values to be in tension with the values presented in the discovery paper, which is very probably due to misuse of the software by the discoverers. The low number of ESPRESSO RV measurements allowed us to derive only the 3σ upper limits for the planet masses, which are $13.71\ M_\oplus$, $9.72\ M_\oplus$, and $26.57\ M_\oplus$ for planets b, c, and d, respectively.

We also investigated the planets from the viewpoint of possible future follow-up observations. First of all, we can conclude that more RV observations are needed to improve the planet masses in this system. The applied spectroscopic observations allowed us to derive precise stellar parameters of the host star and to fit an initial spectroscopic orbit to the RV data, but there is ample room for improvement in this way. We estimated that another 48 ESPRESSO RVs are needed to measure the predicted masses of all planets in HD 22946. planet c could be a suitable target for future atmospheric characterisation via transmission spectroscopy. We can also conclude that planet d as a warm sub-Neptune is very interesting, because there are only a few similar confirmed exoplanets to date. Thanks to the synergy of TESS and CHEOPS missions, there is a growing sample of planets, such as HD 22946d. Such objects are worth investigating in the near future, for example in order to investigate their composition and internal structure. Finally, we can mention that future photometric and/or spectroscopic observations could also be oriented to searching for further possible planets in this system.

References

Akeson, R. L., Chen, X., Ciardi, D., et al. 2013, PASP, 125, 989
Allard, F. 2014, IAU Symp., 299, 271
Badenas-Agusti, M., Günther, M. N., Daylan, T., et al. 2020, AJ, 160, 113
Benz, W., Broeg, C., Fortier, A., et al. 2021, Exp. Astron., 51, 109
Bonfanti, A., Ortolani, S., Piotto, G., & Nascimbeni, V. 2015, A&A, 575, A18
Bonfanti, A., Ortolani, S., & Nascimbeni, V. 2016, A&A, 585, A5
Bonfanti, A., Delrez, L., Hooton, M. J., et al. 2021, A&A, 646, A157
Cacciapuoti, L., Inno, L., Covone, G., et al. 2022, A&A, 668, A85
Castelli, F., & Kurucz, R. L. 2003, IAU Symp., 210, A20
Chen, J., & Kipping, D. 2017, ApJ, 834, 17
Claret, A. 2018, A&A, 618, A20
Claret, A. 2021, RNAAS, 5, 13
Cloutier, R., Doyon, R., Bouchy, F., & Hébrard, G. 2018, AJ, 156, 82
Cooke, B. F., Pollacco, D., & Bayliss, D. 2019, A&A, 631, A83
Cooke, B. F., Pollacco, D., Anderson, D. R., et al. 2021, MNRAS, 500, 5088
Cutri, R. M., Skrutskie, M. F., van Dyk, S., et al. 2003, VizieR Online Data Catalog: II/246
Delrez, L., Ehrenreich, D., Alibert, Y., et al. 2021, Nat. Astron., 5, 775
Dobos, V., Charnoz, S., Pál, A., Roque-Bernard, A., & Szabó, G. M. 2021, PASP, 133, 094401
Dransfield, G., Triaud, A. H. M. J., Guillot, T., et al. 2022, MNRAS, 515, 1328
Foreman-Mackey, D., Agol, E., Ambikasaran, S., & Angus, R. 2017, AJ, 154, 220
Foreman-Mackey, D., Luger, R., Agol, E., et al. 2021, J. Open Source Softw., 6, 3285
Fulton, B. J., Petigura, E. A., Howard, A. W., et al. 2017, AJ, 154, 109
Gaia Collaboration (Brown, A. G. A., et al.) 2021, A&A, 649, A1
Gaia Collaboration (Vallenari, A., et al.) 2023, A&A, in press, https://doi.org/10.1051/0004-6361/202243940
Guerrero, N. M., Seager, S., Huang, C. X., et al. 2021, ApJS, 254, 39
Günther, M. N., & Daylan, T. 2019, Astrophysics Source Code Library [record ascl:1903.003]
Günther, M. N., & Daylan, T. 2021, ApJS, 254, 13
Ho, C. S. K., & Van Eylen, V. 2023, MNRAS, 519, 4056
Hord, B. J., Colón, K. D., Berger, T. A., et al. 2022, AJ, 164, 13
Hoyer, S., Guterman, P., Demangeon, O., et al. 2020, A&A, 635, A24
Kempton, E. M. R., Bean, J. L., Louie, D. R., et al. 2018, PASP, 130, 114401
Kipping, D. 2018, RNAAS, 2, 223
Kipping, D. M., Spiegel, D. S., & Sasselov, D. D. 2013, MNRAS, 434, 1883
Kurucz, R. L. 1993a, SYNTHE spectrum synthesis programs and line data, CD-ROM No. 18 (Cambridge, MA: Smithsonian Astrophysical Observatory)
Kurucz, R. L. 1993b, SYNTHE spectrum synthesis programs and line data (Astrophysics Source Code Library)
Lacedelli, G., Malavolta, L., Borsato, L., et al. 2021, MNRAS, 501, 4148
Lacedelli, G., Wilson, T. G., Malavolta, L., et al. 2022, MNRAS, 511, 4551

Lindegren, L., Bastian, U., Biermann, M., et al. 2021, A&A, 649, A4
Lissauer, J. J., Marcy, G. W., Rowe, J. F., et al. 2012, ApJ, 750, 112
Luque, R., & Pallé, E. 2022, Science, 377, 1211
Marigo, P., Girardi, L., Bressan, A., et al. 2017, ApJ, 835, 77
Martinez, C. F., Cunha, K., Ghezzi, L., & Smith, V. V. 2019, ApJ, 875, 29
Maxted, P. F. L., Ehrenreich, D., Wilson, T. G., et al. 2022, MNRAS, 514, 77
Mayor, M., & Queloz, D. 1995, Nature, 378, 355
Nesvorný, D., & Morbidelli, A. 2008, ApJ, 688, 636
Osborn, H. P., Bonfanti, A., Gandolfi, D., et al. 2022, A&A, 664, A156
Osborn, H. P., Nowak, G., Hébrard, G., et al. 2023, MNRAS, 523, 3069
Otegi, J. F., Bouchy, F., & Helled, R. 2020, A&A, 634, A43
Owen, J. E. 2019, Annu. Rev. Earth Planet. Sci., 47, 67
Pepe, F., Molaro, P., Cristiani, S., et al. 2014, Astron. Nachr., 335, 8
Ricker, G. R. 2014, JAAVSO, 42, 234
Salmon, S. J. A. J., Van Grootel, V., Buldgen, G., Dupret, M. A., & Eggenberger, P. 2021, A&A, 646, A7
Salvatier, J., Wieckiâ, T. V., & Fonnesbeck, C. 2016, Astrophysics Source Code Library [record ascl:1610.016]
Santos, N. C., Sousa, S. G., Mortier, A., et al. 2013, A&A, 556, A150
Scuflaire, R., Théado, S., Montalbán, J., et al. 2008, Ap&SS, 316, 83
Skrutskie, M. F., Cutri, R. M., Stiening, R., et al. 2006, AJ, 131, 1163
Sneden, C. A. 1973, Ph.D. Thesis, The University of Texas at Austin, USA
Sousa, S. G. 2014, in Determination of Atmospheric Parameters of B-, A-, F and G-Type Stars, eds. E. Niemczura, B. Smalley, & W. Pych (Berlin: Springer), 297
Sousa, S. G., Santos, N. C., Israelian, G., Mayor, M., & Monteiro, M. J. P. F. G. 2007, A&A, 469, 783
Sousa, S. G., Santos, N. C., Adibekyan, V., Delgado-Mena, E., & Israelian, G. 2015, A&A, 577, A67
Sousa, S. G., Adibekyan, V., Delgado-Mena, E., et al. 2021, A&A, 656, A53
Stassun, K. G., Oelkers, R. J., Pepper, J., et al. 2018, AJ, 156, 102
Stefánsson, G., Kopparapu, R., Lin, A., et al. 2020, AJ, 160, 259
Steffen, J. H., & Hwang, J. A. 2015, MNRAS, 448, 1956
Szabó, G. M., Gandolfi, D., Brandeker, A., et al. 2021, A&A, 654, A159
Szabó, G. M., Garai, Z., Brandeker, A., et al. 2022, A&A, 659, A7
Tinetti, G., Eccleston, P., Haswell, C., et al. 2021, ArXiv e-prints [arXiv:2104.04824]
Tuson, A., Queloz, D., Osborn, H. P., et al. 2023, MNRAS, 523, 3090
Ulmer-Moll, S., Osborn, H. P., Tuson, A., et al. 2023, A&A, 674, A43
Van Eylen, V., & Albrecht, S. 2015, ApJ, 808, 126
Van Eylen, V., Agentoft, C., Lundkvist, M. S., et al. 2018, MNRAS, 479, 4786
Van Eylen, V., Albrecht, S., Huang, X., et al. 2019, AJ, 157, 61
Weiss, L. M., Marcy, G. W., Petigura, E. A., et al. 2018, AJ, 155, 48
Wilson, T. G., Goffo, E., Alibert, Y., et al. 2022, MNRAS, 511, 1043
Wright, E. L., Eisenhardt, P. R. M., Mainzer, A. K., et al. 2010, AJ, 140, 1868

[1] MTA-ELTE Exoplanet Research Group, 9700 Szombathely, Szent Imre h. u. 112, Hungary
e-mail: zgarai@ta3.sk
[2] ELTE Gothard Astrophysical Observatory, 9700 Szombathely, Szent Imre h. u. 112, Hungary
[3] Astronomical Institute, Slovak Academy of Sciences, 05960 Tatranská Lomnica, Slovakia
[4] Physikalisches Institut, University of Bern, Gesellsschaftstrasse 6, 3012 Bern, Switzerland
[5] Department of Physics and Kavli Institute for Astrophysics and Space Research, Massachusetts Institute of Technology, Cambridge, MA 02139, USA
[6] Dipartimento di Fisica, Universita degli Studi di Torino, via Pietro Giuria 1, 10125, Torino, Italy
[7] Department of Astronomy, Stockholm University, AlbaNova University Center, 10691 Stockholm, Sweden
[8] Instituto de Astrofisica e Ciencias do Espaco, Universidade do Porto, CAUP, Rua das Estrelas, 4150-762 Porto, Portugal
[9] Astrophysics Group, Cavendish Laboratory, University of Cambridge, J.J. Thomson Avenue, Cambridge CB3 0HE, UK
[10] Astrobiology Research Unit, Université de Liège, Allée du Six-Août 19C, 4000 Liège, Belgium
[11] Space Research Institute, Austrian Academy of Sciences, Schmiedlstrasse 6, 8042 Graz, Austria

[12] Observatoire Astronomique de l'Université de Genève, Chemin Pegasi 51, Versoix, Switzerland

[13] Centre for Exoplanet Science, SUPA School of Physics and Astronomy, University of St Andrews, North Haugh, St Andrews KY16 9SS, UK

[14] Space Research Institute, Austrian Academy of Sciences, Schmiedlstrasse 6, 8042 Graz, Austria

[15] INAF, Osservatorio Astronomico di Padova, Vicolo dell'Osservatorio 5, 35122 Padova, Italy

[16] Department of Astrophysics, University of Vienna, Tuerkenschanzstrasse 17, 1180 Vienna, Austria

[17] Institute of Planetary Research, German Aerospace Center (DLR), Rutherfordstrasse 2, 12489 Berlin, Germany

[18] European Space Agency (ESA), European Space Research and Technology Centre (ESTEC), Keplerlaan 1, 2201 AZ Noordwijk, The Netherlands

[19] Instituto de Astrofisica de Canarias, 38200 La Laguna, Tenerife, Spain

[20] Institut d'Estudis Espacials de Catalunya (IEEC), 08034 Barcelona, Spain

[21] Depto. de Astrofisica, Centro de Astrobiologia (CSIC-INTA), ESAC campus, 28692 Villanueva de la Cañada (Madrid), Spain

[22] Université Grenoble Alpes, CNRS, IPAG, 38000 Grenoble, France

[23] Université de Paris, Institut de physique du globe de Paris, CNRS, 75005 Paris, France

[24] Departamento de Fisica e Astronomia, Faculdade de Ciencias, Universidade do Porto, Rua do Campo Alegre, 4169-007 Porto, Portugal

[25] Center for Space and Habitability, University of Bern, Gesellschaftsstrasse 6, 3012 Bern, Switzerland

[26] Leiden Observatory, University of Leiden, PO Box 9513, 2300 RA Leiden, The Netherlands

[27] Department of Space, Earth and Environment, Chalmers University of Technology, Onsala Space Observatory, 43992 Onsala, Sweden

[28] Space sciences, Technologies and Astrophysics Research (STAR) Institute, Université de Liège, 19C Allée du Six-Août, 4000 Liège, Belgium

[29] Departamento de Astrofisica, Universidad de La Laguna, 38206 La Laguna, Tenerife, Spain

[30] Institut de Ciencies de l'Espai (ICE, CSIC), Campus UAB, Can Magrans s/n, 08193 Bellaterra, Spain

[31] Aix–Marseille Univ., CNRS, CNES, LAM, 38 rue Frédéric Joliot-Curie, 13388 Marseille, France

[32] IMCCE, UMR8028 CNRS, Observatoire de Paris, PSL Univ., Sorbonne Univ., 77 av. Denfert-Rochereau, 75014 Paris, France

[33] Max Planck Institute for Extraterrestrial Physics, Giessenbachstrasse 1, 85748 Garching bei München, Germany

[34] Dipartimento di Fisica e Astronomia "Galileo Galilei", Universita degli Studi di Padova, Vicolo dell'Osservatorio 3, 35122 Padova, Italy

[35] INAF, Osservatorio Astrofisico di Catania, Via S. Sofia 78, 95123 Catania, Italy

[36] Astrophysics Group, Keele University, Staffordshire ST5 5BG, UK

[37] Admatis, 5. Kandó Kálmán Street, 3534 Miskolc, Hungary

[38] Konkoly Observatory, Research Centre for Astronomy and Earth Sciences, 1121 Budapest, Konkoly Thege Miklós út 15–17, Hungary

[39] Institut d'astrophysique de Paris, UMR7095 CNRS, Université Pierre-et-Marie-Curie, 98bis blvd. Arago, 75014 Paris, France

[40] Centre for Mathematical Sciences, Lund University, Box 118, 22100 Lund, Sweden

[41] Department of Physics, University of Warwick, Gibbet Hill Road, Coventry CV4 7AL, UK

[42] Center for Astronomy and Astrophysics, Technical University Berlin, Hardenberstrasse 36, 10623 Berlin, Germany

[43] Institute of Astronomy, University of Cambridge, Madingley Road, Cambridge CB3 0HA, UK

[44] INAF, Osservatorio Astrofisico di Torino, Via Osservatorio 20, 10025 Pino Torinese, TO, Italy

[45] Department of Space and Climate Physics, Mullard Space Science Laboratory, Holmbury St Mary RH5 6NT, UK

[46] Brorfelde Observatory, Observator Gyldenkernes Vej 7, 4340 Tøl-løse, Denmark

Appendix A: Additional tables

Table A.1. Best-fitting GP hyperparameters and detrending parameters.

Parameter [unit]	Description	Value$^{+1\sigma}_{-1\sigma}$
$\log \sigma_{\mathrm{CHEOPS}}$ [ppt]	log of scatter in the CHEOPS data	$-2.384^{+0.057}_{-0.061}$
$\log \sigma_{\mathrm{TESS}}$ [ppt]	log of scatter in the TESS data	$-2.845^{+0.024}_{-0.023}$
$\varphi_{\omega_0,\mathrm{CHEOPS}}$ [1/deg]	typical frequency of variation in the shared CHEOPS roll-angle GP	$1.70^{+0.19}_{-0.16}$
$\omega_{0,\mathrm{TESS}}$ [1/d]	frequency for the TESS SHOTerm GP kernel	$1.87^{+0.10}_{-0.09}$
$\varphi_{S_0,\mathrm{CHEOPS}}$	scaled power in the shared CHEOPS roll-angle GP	$0.0062^{+0.0010}_{-0.0009}$
$S_{0,\mathrm{TESS}}$	scaled power in the TESS SHOTerm GP kernel	$0.0066^{+0.0010}_{-0.0008}$
$\varphi_{\mathrm{power},\mathrm{CHEOPS}}$	power in the shared CHEOPS roll-angle GP	$0.052^{+0.020}_{-0.013}$
$\varphi_{\mathrm{lengthscale},\mathrm{CHEOPS}}$ [deg]	typical lengthscale of variation in the shared CHEOPS rollangle GP	$3.68^{+0.38}_{-0.37}$
$df/d(\mathrm{time})_{\mathrm{1st,CHEOPS}}$	linear detrending parameter for time trend vs. flux – 1st CHEOPS visit	0.075 ± 0.011
$df/d(\mathrm{bg})_{\mathrm{1st,CHEOPS}}$	linear detrending parameter for background vs. flux – 1st CHEOPS visit	-0.026 ± 0.036
$d^2f/d(\mathrm{bg})^2_{\mathrm{1st,CHEOPS}}$	quadratic detrending parameter for background vs. flux – 1st CHEOPS visit	0.0278 ± 0.0025
$df/d(\mathrm{centroid\ x})_{\mathrm{1st,CHEOPS}}$	linear detrending parameter for x centroid vs. flux – 1st CHEOPS visit	$0.0386^{+0.0080}_{-0.0078}$
$df/d(\mathrm{centroid\ y})_{\mathrm{1st,CHEOPS}}$	linear detrending parameter for y centroid vs. flux – 1st CHEOPS visit	$-0.0458^{+0.0083}_{-0.0084}$
$df/d(\mathrm{centroid\ x})_{\mathrm{2nd,CHEOPS}}$	linear detrending parameter for x centroid vs. flux – 2nd CHEOPS visit	$0.202^{+0.044}_{-0.045}$
$d^2f/d(\mathrm{centroid\ x})^2_{\mathrm{2nd,CHEOPS}}$	quadratic detrending parameter for x centroid vs. flux – 2nd CHEOPS visit	-0.0304 ± 0.0083
$df/d(\mathrm{time})_{\mathrm{3rd,CHEOPS}}$	linear detrending parameter for time trend vs. flux – 3rd CHEOPS visit	0.015 ± 0.010
$df/d(\mathrm{centroid\ y})_{\mathrm{3rd,CHEOPS}}$	linear detrending parameter for y centroid vs. flux – 3rd CHEOPS visit	$-0.0357^{+0.0074}_{-0.0075}$
$df/d(\mathrm{time})_{\mathrm{4th,CHEOPS}}$	linear detrending parameter for time trend vs. flux – 4th CHEOPS visit	0.103 ± 0.013
$df/d(\mathrm{centroid\ y})_{\mathrm{4th,CHEOPS}}$	linear detrending parameter for y centroid vs. flux – 4th CHEOPS visit	-0.061 ± 0.010
$d^2f/d(\mathrm{centroid\ y})^2_{\mathrm{4th,CHEOPS}}$	quadratic detrending parameter for y centroid vs. flux – 4th CHEOPS visit	0.0086 ± 0.0019
$x_{\mathrm{mean,1st,CHEOPS}}$ [ppt]	the average offset of the median-normalised flux – 1st CHEOPS visit	0.007 ± 0.011
$x_{\mathrm{mean,2nd,CHEOPS}}$ [ppt]	the average offset of the median-normalised flux – 2nd CHEOPS visit	0.066 ± 0.011
$x_{\mathrm{mean,3rd,CHEOPS}}$ [ppt]	the average offset of the median-normalised flux – 3rd CHEOPS visit	0.039 ± 0.010
$x_{\mathrm{mean,4th,CHEOPS}}$ [ppt]	the average offset of the median-normalised flux – 4th CHEOPS visit	0.314 ± 0.014
$x_{\mathrm{mean,5th,CHEOPS}}$ [ppt]	the average offset of the median-normalised flux – 5th CHEOPS visit	0.061 ± 0.011
$x_{\mathrm{mean,TESS}}$ [ppt]	the average offset of the median-normalised flux in TESS data	$0.0179^{+0.0085}_{-0.0084}$

Notes. Based on the joint fit of the TESS and CHEOPS photometric data, and RV observations. The table shows the best-fitting value of the given parameter and its $\pm 1\sigma$ uncertainty. The fitted values correspond to quantile 0.50 (median) and the uncertainties to quantils ± 0.341 in the parameter distributions obtained from the samples.

Table A.2. As in Table A.1, but for model posteriors of the host HD 22946.

Parameter [unit]	Description	Value$^{+1\sigma}_{-1\sigma}$
T_{eff} [K]	effective temperature	6167^{+64}_{-63}
$\log g$ [cgs]	log of surface gravity	4.358 ± 0.016
$u_{1,\mathrm{TESS}}$	quadratic LD coefficient	0.196 ± 0.077
$u_{2,\mathrm{TESS}}$	quadratic LD coefficient	0.244 ± 0.086
$u_{1,\mathrm{CHEOPS}}$	quadratic LD coefficient	$0.346^{+0.081}_{-0.079}$
$u_{2,\mathrm{CHEOPS}}$	quadratic LD coefficient	$0.291^{+0.089}_{-0.090}$
R_{s} [$R_\odot$]	stellar radius	$1.1161^{+0.0088}_{-0.0089}$
M_{s} [$M_\odot$]	stellar mass	1.105 ± 0.038
γ [m s^{-1}]	system RV	$16\,854.48^{+0.82}_{-0.76}$